Proceedings of the ASME 2019
Dynamic Systems and Control Conference
DSCC 2019
October 8-11, 2019, Park City, Utah, USA

DSCC2019-9118

ON THE DYNAMICS AND CONTROL OF A FULL WRIST EXOSKELETON FOR TREMOR ALLEVIATION

Jiamin Wang, Oumar Barry*, Andrew J. Kurdila
Department of Mechanical Engineering
Virginia Polytechnic Institute and State University
Blacksburg, Virginia 24061

Sujith Vijayan
School of Neuroscience
Virginia Polytechnic Institute and State University
Blacksburg, Virginia 24061

ABSTRACT

This paper introduces a novel wearable full wrist exoskeleton designed for the alleviation of tremor in patients suffering from Parkinson's Disease and Essential Tremor. The design introduces a structure to provide full observation of wrist kinematics as well as actuation in wrist flexion/extension and radial/ulnar deviation. To examine the feasibility of the design, the coupled dynamics of the device and the forearm is modeled via a general multibody framework. The dynamic analysis considers human motion, wrist stiffness, and tremor dynamics. The analysis of the model reveals that the identification of the wrist kinematics is indispensable for the controller design. Nonlinear regression based on the Levenberg-Marquardt algorithm has been applied to estimate the unknown parameters in a kinematic structural function designed to approximate the wrist kinematics, which leads to the construction of the control system framework. Finally, several simulation cases are demonstrated to conclude the study.

NOMENCLATURE

The mathematical notions used are listed as following:

$\|Z\|_n$ The induced n-norm of a matrix Z ($n = 2$ if not specified)
$z_1 \times z_2$ Multiplications of quaternions z_1 (4×1) and z_2 (4×1)
$\bar{z}$ Conjugation of quaternion z (4×1)
$z_{m \times n}$ A $m \times n$ matrix with all elements as $z \in \mathbb{R}$ (fits along with its neighboring blocks if no dimension specified)
I_n Identity matrix of a specific dimension n (fits along with its neighboring blocks if no dimension specified)
$Z > 0$ Square matrix Z is positive definite
Z^{-T} The transposed inverse of Z (since $(Z^{-1})^T = (Z^T)^{-1}$)

1 INTRODUCTION

Millions of people all around the world suffer from pathological tremor caused by neurological disorders including Essential Tremor [1] and Parkinson's Disease [2, 3]. A common symptom of most of these tremors is the uncontrollable shaking of limbs, which significantly undermines the quality of life of patients. Especially for Parkinson's Disease, since the majority of the patients come from the aged population, the effect of tremor may also pose potential life danger (due to slipping, falling [4], etc.). These concerns provide motivation for researchers all over the world to find solutions to these illnesses in order to improve the lives of these patients.

In addition to medication and surgery, various medical devices have been developed to help relieve patients from their difficulties. As a result of breakthroughs in mechatronic and robotic technologies, rehabilitation devices including orthosis and exoskeletons [5] are gaining popularity in recent years. In general, active robotic devices offer more possible solutions than passive devices as they are more versatile and adaptive, and they can intrinsically interface humans and hardware. For the upper limb (elbow, forearm, wrist, etc.), active orthosis and exoskeletons including DRIFTS [6], WOTAS [7], and work led by Huen [8] have been successful in reducing tremors. Most of these devices adopt a similar framework of human motion estimation. As tremors are generally considered rhythmic and roughly sinusoidal [9], the voluntary and tremorous movements are extracted

*Email: obarry@vt.edu

and separated from the motion recorded from the sensor (IMU, EMG, etc.) with filters such as Weighted Fourier Linear Combiner (WFLC) [10] and Extended Kalman Filter (EKF) [11]. Voluntary or intended motion estimation will be used in this work as the reference for the various possible controller setups, i.e., passive impedance control and active vibration cancelling [7, 10].

Human wrists have delicate and sophisticated structures. Located at the end of the human arm, the wrist joint is crucial to object manipulation. A wrist joint has two degrees of freedom (DOF), namely flexion/extension motion (FE) and radial/ulnar deviation motion (RUD). The approximate location of the axes of these motions are demonstrated in Fig. 1. Realizing full wrist tremor control in both motions is a challenging task, since the kinematics and dynamics of the hand are affected by the coupling of the two DOFs of the wrist joint [12]. Different users also have different wrist kinematic profiles. As some Parkinson's Disease patients also suffer muscle deformations [13], a device may be limited if it is designed based on a standard wrist profile. Finally, in addition to the offset between the rotation axes [14], both motions may not even be pure rotations (i.e. with no coupled translations) that have fixed axes positioned on the wrist. Almost none of the previous work on tremor control devices has considered tremor in the RUD motion. This motivates us to explore the possibility of a novel framework to provide a solution for full wrist tremor control.

In this paper, we introduce the development of a novel full wrist exoskeleton for tremor control. The design structure of the rigid link tremor alleviating wrist exoskeleton - TAWE is presented in Sec.2. The objective of the design is to fulfill the functionalities:

(O1) Wrist kinematics and tremor data collection and assessment with a variety of sensors.

(O2) Tremor suppression control and light power augmentation of the full wrist with the two actuators.

A contribution of the paper is the detailed multibody modeling and analysis of the coupled forearm-exoskeleton system, which are explained in Sec.3, in which the human motion, stiffness and tremor dynamics are considered. The study on the dynamics has indicated the necessity of acquiring the unknown wrist kinematic model in order to realize controller design. The approach of wrist kinematic identification and its preliminary validation in simulation environment is then introduced in Sec.4. The control framework is presented in Sec.5, where the characteristics of the controller is studied with two simulation cases namely power augmentation and tremor suppression. Finally, Sec.6 concludes the study and proposes future research works.

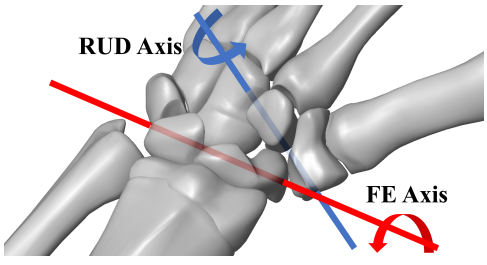

FIGURE 1: Approximate locations of FE and RUD rotation axes [14] on the wrist of a left forearm.

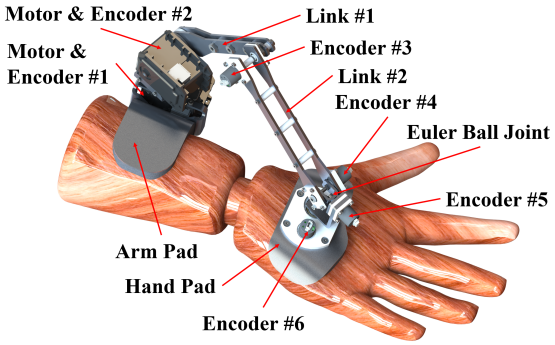

FIGURE 2: The CAD model of TAWE attached to a right forearm

2 The Exoskeleton Design and Its Kinematics

The Tremor Alleviating Wrist Exoskeleton (TAWE) is a 6-DOF exoskeleton for full wrist tremor assessment and control. The 3D model of the prototype designed for the right-hand wrist is presented in Fig.2. The weight of the device (excluding the attachment pads) is approximately 485 grams. The two attachment pads are assumed to be firmly fixed on front forearm (slightly behind the wrist) and the back of the hand, respectively. The device consists of two main subsystems - the linkage and the ball joint. The linkage subsystem has three rotational DOFs measured by the absolute encoders (US Digital MAE3). Two of the DOFs close to the attachment pad are actuated by servo motors (Dynamixel MX-28). The end point of the linkage subsystem (on Link #2) is attached to the ball joint subsystem. The naming of the Euler Ball Joint indicates that the 3D rotation of the ball joint is realized with Euler angle rotations, which allows the installation of encoders to measure the 3D rotation. The IMU sensors will be fixed on the attachment pads, while the other electronic components (EMG sensors, batteries, etc.) are hidden in the current figure.

The dimensions of the design are determined by the kinematic workspace of the wrist. The locations of the attachment pads and the lengths of the linkages are carefully selected so that the geometric reachability of the linkage subsystem is guaranteed over the design motion envelope. In the current design, the length of each link is 12 cm. A big challenge of the design is to avoid the singularity in the Euler Ball Joint, which occurs when the rotation along an axis results in the colinearity of the other two axes. While an optimal systematic design framework will be explored in future research, the current design is feasible for the selected forearm model where the FE and RUD axes intersect. As shown in Fig.3, TAWE is able to reach extreme poses. No geometric interference is experienced in the selected workspace

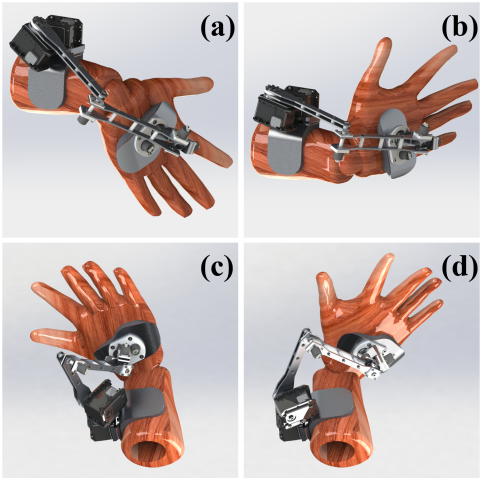

FIGURE 3: TAWE at rotation limits - (a): flexion: 75°, radial deviation: 20°; (b): flexion: 75°, ulnar deviation: 45°; (c): extension: 75°, radial deviation: 20°; (d): extension: 75°, ulnar deviation: 45°.

of -75°∼ 75°in FE and -20°∼ 45°in RUD.

When the exoskeleton is attached to the arm, a closed kinematic chain is formed from the open kinematic chain of the two subsystems. As shown in Fig.4, the two kinematic chains are connected at Frame #1 and Frame #5. As mentioned in Sec.1, the forearm kinematic chain is generally assumed to be unknown. On the other hand, the TAWE kinematic chain can be easily represented with the homogeneous transformation matrices $T_{i,j}$ (from frame #i to frame #j) which is defined along with its inverse as

$$T_{i,j} = \begin{bmatrix} R & d \\ 0_{1\times 3} & 1 \end{bmatrix} = T_{j,i}^{-1}; \quad T_{j,i} = \begin{bmatrix} R^T & -R^T d \\ 0_{1\times 3} & 1 \end{bmatrix} \tag{1}$$

where $R \in \mathbb{R}^{3\times 3}$ and $d \in \mathbb{R}^3$ are the rotation matrix and translational displacement from Frame #i to Frame #j, respectively. The transformations between the frames in the exoskeleton kinematic chain are demonstrated in Table 1. Here, the terms marked as $d_{k,i}$ and $R_{k,i}$ respectively stand for the translation and rotation along the k axis in Frame #i. By defining $\theta_W = [\theta_{W,1}, \theta_{W,2}]^T \in \mathbb{R}^2$ as the wrist angular displacement and $\theta_E = [\theta_{E,1}, \theta_{E,2}, \theta_{E,3}, \theta_{E,4}, \theta_{E,5}, \theta_{E,6}]^T \in \mathbb{R}^6$ as the angular displacement at the six rotation axes, respectively, the translational and rotational terms $R_{z,1}$, $R_{x,2}$, $R_{x,3}$, R_4, d_w, and R_w are state dependent. The rest of the terms are constant kinematic transformations. Furthermore, d_w and R_w are assumed to be unknown and cannot be directly measured with sensors.

Observe that the transformation from Frame #1 to Frame #4 will allow the linkage subsystem to reach any point in the 3D spherical space with a radius of $d_{y,3} + d_{y,4}$ centered at the origin of Frame #3. The Euler Ball joint realizes the attitude consistency between the end of the linkage and the hand attachment pad. From the multibody perspective, such a 6-DOF kinematic

TABLE 1: THE HOMOGENEOUS TRANSFORMATIONS ON THE EXOSKELETON KINEMATIC CHAIN

From	To	Translation (d)	Rotation (R)
#1	#2	d_1	$R_{z,1}(\theta_{E,1})R_1$
#2	#3	$d_{z,2}$	$R_{x,2}(\theta_{E,2})$
#3	#4	$d_{y,3}$	$R_{x,3}(\theta_{E,3})$
#4	#5	$d_{y,4}$	$R_4(\theta_{E,4}, \theta_{E,5}, \theta_{E,6})$
#1	#6	$d_w(\theta_{W,1}, \theta_{W,2})$	$R_w(\theta_{W,1}, \theta_{W,2})$
#6	#5	d_5	R_5

structure can connect any two 3D bodies within its range, which explains why TAWE can connect the forearm and hand regardless of the unknown wrist kinematics. This also allows the wrist of the user to operate freely with no spatial restriction.

3 Dynamical Modeling and Analysis

While the design of TAWE is explained in the previous section, the feasibility of realization of this exoskeleton is not yet guaranteed. A major concern is whether a controller can be successfully designed for suppressing coupled tremor at the wrist. This requires us to perform a multibody dynamic analysis of the forearm-exoskeleton system. To fully analyze the system, both systems are modeled as floating base systems that are connected with constraints. Since the human arm is not a rigid body system, a few model assumptions are made:

(A1) The forearm is approximated as a rigid body model, where the deformation of the muscles are omitted.
(A2) Muscle actuation forces are generalized into direct torque inputs at the joint directions.
(A3) The supination motion of the forearm is fixed in this study.

Based on these assumptions, by modeling the forearm as a floating base system whose base coordinate frame is Frame #1 , its dynamic model can be represented in the form of nonholonomic

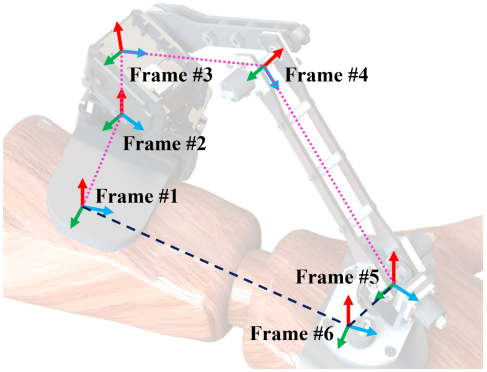

FIGURE 4: The close kinematic chain and coordinate frames of the forearm-exoskeleton system (green arrow: x axis; blue arrow: y axis; red arrow: z axis; dot line: exoskeleton kinematic chain; dash line: forearm kinematic chain.)

equations

$$M_1(q_1,\xi_1)\ddot{q}_1 = H_1(q_1,\dot{q}_1,\xi_1) + J_{u_1}^T(q_1,\xi_1)u_1 + W_1^T(q_1,\xi_1)w_1 \quad (2a)$$

$$\dot{\xi}_1 = J_{\xi_1}(q_1,\xi_1)\dot{q}_1 \quad (2b)$$

where

$$\dot{q}_1 = \begin{bmatrix}\dot{\theta}_1^T & v_1^T & \omega_1^T\end{bmatrix}^T$$

is the derivative of the generalized coordinates, which includes the float base translational velocity $v_1 \in \mathbb{R}^3$ in the global frame, the float base angular velocity $\omega_1 \in \mathbb{R}^3$ in the local base frame, and the wrist joints $\theta_1 = \theta_W$; $\xi_1 \in \mathbb{R}^4$ is the quaternion vector of base orientation, which is nonholonomic and therefore separated from Eq.(2a); $u_1 \in \mathbb{R}^8$ is the input exerted at the float-base coordinates and the wrist joint; w_1 is the disturbance/perturbation exerted at each generalized coordinate; $M_1 \in \mathbb{R}^{8\times8}$ is the inertia matrix; $H_1 \in \mathbb{R}^8$ is the system internal generalized force that includes Coriolis, centripetal and damping forces; $J_{u_1} \in \mathbb{R}^{8\times8}$ and $W_1 \in \mathbb{R}^{8\times8}$ are the Jacobian matrices for u_1 and w_1 respectively; and $J_{\xi_1} \in \mathbb{R}^{4\times8}$ is the Jacobian matrix for ξ_1, which is shown in reference [15] to be

$$\dot{\xi}_1 = \frac{1}{2}\xi_1 \times \begin{bmatrix}0 & \omega_1^T\end{bmatrix}^T. \quad (3)$$

Next, the dynamic model of the exoskeleton is considered, which has a structure similar to Eq.(2). For convenience, this subsystem is also based at Frame #1. During the modeling, since the Euler Ball Joint has relatively small inertia, $\theta_{E,4}, \theta_{E,5}, \theta_{E,6}$ are omitted in the modeling process, which results in simplifying the ball joint as a point. As a result, the EOM of the system can be written as

$$M_2(q_2,\xi_2)\ddot{q}_2 = H_2(q_2,\dot{q}_2,\xi_2) + J_{u_2}^T(q_2,\xi_2)u_2 \quad (4a)$$

$$\dot{\xi}_2 = J_{\xi_2}(q_2,\xi_2)\dot{q}_2 \quad (4b)$$

where

$$\dot{q}_2 = \begin{bmatrix}\dot{\theta}_2^T & v_2^T & \omega_2^T\end{bmatrix}^T$$

is the derivative of the generalized coordinate q_2 of the system, consisting of the base translational velocity $v_2 \in \mathbb{R}^3$ in the global frame, the base angular velocity $\omega_2 \in \mathbb{R}^3$ in the local base frame, and the linkage subsystem joints $\theta_2 = [\theta_{E,1}, \theta_{E,2}, \theta_{E,3}]^T \in \mathbb{R}^3$; and $u_2 \in \mathbb{R}^2$ is the exoskeleton actuation input. The definition of the other variables are similar to that in Eq.(2), except that the disturbance/perturbation terms are omitted.

3.1 Coupling of Subsystem Dynamics

The combination of the two models can be achieved with the introduction of constraints in the following nonholonomic form

$$\dot{r}_\lambda = J_\lambda(q,\xi)\dot{q} \quad (5)$$

where

$$q = \begin{bmatrix}q_1^T & q_2^T\end{bmatrix}^T; \quad \xi = \begin{bmatrix}\xi_1^T & \xi_2^T\end{bmatrix}^T \quad (6)$$

are the combined generalized coordinate and nonholonomic state vectors respectively; $r_\lambda \in \mathbb{R}^9$ is the constraint value vector, which is set to $r_\lambda = 0$ for time invariant constraints; and $J_\lambda \in \mathbb{R}^{9\times17}$ is the constraint Jacobian matrix. The expression of r_λ are

$$r_\lambda = \begin{bmatrix}\rho_{1,1} - \rho_{1,2} \\ \begin{bmatrix}0_{3\times1} & I_3\end{bmatrix}(\xi_1 \times \bar{\xi}_2) \\ \rho_{5,1} - \rho_{5,2}\end{bmatrix} \quad (7)$$

where $\rho_{1,1} = \begin{bmatrix}0_{3\times2} & I_3 & 0_{3\times3}\end{bmatrix} q_1$ and $\rho_{1,2} = \begin{bmatrix}0_{3\times3} & I_3 & 0_{3\times3}\end{bmatrix} q_2$ are the base positions of each subsystems; and

$$\rho_{5,1} = \begin{bmatrix}I_3 & 0_{3\times1}\end{bmatrix} T_{1,2}T_{2,3}T_{3,4}T_{4,5} \begin{bmatrix}0_{1\times3} & 1\end{bmatrix}^T$$

$$\rho_{5,2} = \begin{bmatrix}I_3 & 0_{3\times1}\end{bmatrix} T_{1,6}T_{6,5} \begin{bmatrix}0_{1\times3} & 1\end{bmatrix}^T$$

are the relative positions of the origin of Frame #5 with respect to Frame #1 in each subsystem's base frame. Furthermore, with respect to the states, the constraint Jacobian matrix can be divided into parts as

$$J_\lambda = \begin{bmatrix}J_{\lambda_1} & J_{\lambda_2}\end{bmatrix} \quad (8)$$

where $J_{\lambda_1} \in \mathbb{R}^{9\times8}$ is the part of the Jacobian matrix with respect to q_1; and $J_{\lambda_2} \in \mathbb{R}^{9\times9}$ is the part with respect to q_2. Since there is no internal constraints in any subsystems, it is required that J_{λ_2} has full rank. Furthermore, since the first six row of r_λ only involves the v and ω from the bases, and the rest only involves θ_1 and θ_2, the Jacobian matrix can be further specified as

Since the exoskeleton is fully constrained with respect to the forearm, the constraints in Eq.(5) imply that the kinematics of exoskeleton (q_2, $\dot{q}_2$ and ξ_2) can be fully expressed in terms of q_1, $\dot{q}_1$ and ξ_1. This leads to

$$\dot{q}_2 = -J_{\lambda_2}^{-1}J_{\lambda_1}\dot{q}_1; \quad \xi_2 = \xi_1 \quad (9)$$

where $J_{\lambda_2}^{-1}J_{\lambda_1}$ can be calculated based on the previous setup as

$$J_{\lambda_2}^{-1}J_{\lambda_1} = \begin{bmatrix}J_{\lambda_{2,s}}^{-1}J_{\lambda_{1,s}} & 0_{3\times6} \\ 0_{6\times2} & J_{\lambda_{2,r}}^{-1}J_{\lambda_{1,r}}\end{bmatrix}. \quad (10)$$

Differentiating the constraint equation with respect to time yields

$$\ddot{q}_2 = -J_{\lambda_2}^{-1}(J_{\lambda_1}\ddot{q}_1 + \dot{J}_{\lambda_1}\dot{q}_1 - \dot{J}_{\lambda_2}J_{\lambda_2}^{-1}J_{\lambda_1}\dot{q}_1). \quad (11)$$

Therefore, the dynamics between the two subsystems can be coupled by preserving the generalized coordinates of the forearm. Based on the constrained arm subsystem

$$M_1\ddot{q}_1 = H_1 + J_{u_1}^T u_1 + W_1^T w_1 + J_{\lambda_1}^T \lambda, \quad (12)$$

and by calculating the constraint force

$$\lambda = -J_{\lambda_2}^{-T}(M_2J_{\lambda_2}^{-1}(J_{\lambda_1}\ddot{q}_1 + \dot{J}_{\lambda_1}\dot{q}_1 - \dot{J}_{\lambda_2}J_{\lambda_2}^{-1}J_{\lambda_1}\dot{q}_1) + H_2 + J_{u_2}^T u_2), \quad (13)$$

the combined multibody system with the generalized coordinate

as q_1 can be calculated as

$$\begin{aligned}(M_1+&J_{\lambda_1}^T J_{\lambda_2}^{-T} M_2 J_{\lambda_2}^{-1} J_{\lambda_1})\ddot{q}_1 \\ &= H_1 + J_{u_1}^T u_1 + W_1^T w_1 - J_{\lambda_1}^T J_{\lambda_2}^{-T} H_2 - J_{\lambda_1}^T J_{\lambda_2}^{-T} J_{u_2}^T u_2 \\ &\quad - J_{\lambda_1}^T J_{\lambda_2}^{-T} M_2 J_{\lambda_2}^{-1} (\dot{J}_{\lambda_1}\dot{q}_1 - \dot{J}_{\lambda_2} J_{\lambda_2}^{-1} J_{\lambda_1}\dot{q}_1) \qquad (14a)\end{aligned}$$

$$\dot{\xi}_1 = J_{\xi_1}(q_1, \xi_1)\dot{q}_1. \qquad (14b)$$

Since M_1 and M_2 are positive definite, this results in a new inertia matrix $M_u = M_1 + J_{\lambda_1}^T J_{\lambda_2}^{-T} M_2 J_{\lambda_2}^{-1} J_{\lambda_1}$ that is also positive definite. The new multibody system is therefore used for the following analysis.

3.2 Free Base Model

For human motion, muscle actuation is often modeled from inputs generated by a neural motion controller based on a planned trajectory. Here two more model assumptions are made to limit the scope of the study and take human motion into consideration:

(A4) The human muscle controller can adapt to the system inertia (including the exoskeleton and external load) and internal forces.

(A5) The human muscle controller consists of an inverse dynamics feed-forward controller and a feedback controller.

Again, the 8-DOF system can be fully actuated with the control muscle input u_1. It is reasonable to define the output as

$$\dot{y}_1 = J_h(x)\dot{q}_1; \quad \ddot{y}_1 = J_h(x)\ddot{q}_1 + \dot{J}_h(x)\dot{q}_1; \qquad (15)$$

with

$$J_h = \begin{bmatrix} I_5 & 0_{5\times 3} \\ 0_{3\times 5} & J_{h_\xi}(q_1, \xi) \end{bmatrix}$$

where $J_{h_\xi} \in \mathbb{R}^{3\times 3}$ is the Jacobian from the quaternion attitude controller

$$y_\xi = \begin{bmatrix} 0_{3\times 1} & I_3 \end{bmatrix} (\xi_1 \times \bar{\xi}_{1_r}(t)) \qquad (16)$$

Here, $\xi_{1_r} : \mathbb{R}_+ \to \mathbb{R}^4$ is the quaternion reference. Furthermore, the output reference can be defined as

$$r_h = \begin{bmatrix} \theta_{W_r}^T(t) & \rho_{1_r}^T(t) & 0_{1\times 3} \end{bmatrix}^T \qquad (17)$$

where $\theta_{W_r} : \mathbb{R}_+ \to \mathbb{R}^2$ is the wrist joint reference function; and $\rho_{1_r} : \mathbb{R}_+ \to \mathbb{R}^3$ is the forearm translational position reference function. These setups lead to the muscle control input

$$\begin{aligned}u_1 = J_{u_1}^{-T} \big(M_u J_h^{-1} (\ddot{r}_h - \dot{J}_h \dot{q}_1 + \Psi_1) + H_0(x) - \ H_1 + J_{\lambda_1}^T J_{\lambda_2}^{-T} H_2 \\ + J_{\lambda_1}^T J_{\lambda_2}^{-T} M_2 J_{\lambda_2}^{-1} (\dot{J}_{\lambda_1}\dot{q}_1 - \dot{J}_{\lambda_2} J_{\lambda_2}^{-1} J_{\lambda_1}\dot{q}_1) \big) \qquad (18)\end{aligned}$$

Here, $\Psi_1 \in \mathbb{R}^8$ is feedback control term; and $H_0 : \mathbb{R}^{42} \to \mathbb{R}^8$ is the uncompensated internal force. Therefore, by defining the error as

$$e_1 = \begin{bmatrix} e_{1,p}^T & e_{1,d}^T \end{bmatrix}^T = \begin{bmatrix} (y_1 - r_h)^T & (\dot{y}_1 - \dot{r}_h)^T \end{bmatrix}^T \qquad (19)$$

under the muscle control input, the control system can be updated as

$$M_u J_h^{-1} \dot{e}_{1,d} = M_u J_h^{-1} \Psi_1 + H_0 + W_1^T w - J_{\lambda_1}^T J_{\lambda_2}^{-T} J_{u_2}^T u_2 \qquad (20)$$

Currently the study focuses on the control of tremor at the wrist. By defining the wrist control error

$$e = \begin{bmatrix} e_p^T & e_d^T \end{bmatrix}^T = \begin{bmatrix} (\theta_1 - \theta_{W_r})^T & (\dot{\theta}_1 - \dot{\theta}_{W_r})^T \end{bmatrix}^T, \qquad (21)$$

and with the declaration of the selection matrices $J_s = [I_2,\ 0_{2\times 6}]$ and $J_c = [0_{6\times 2},\ I_6]$, the inertia matrix can be segmented as

$$M_u = \begin{bmatrix} M_s & M_c \\ M_c^T & M_r \end{bmatrix}; \quad M_s = J_s M_u J_s^T; \quad M_r = J_r M_u J_r^T; \qquad (22)$$

As a result, the final wrist error system can be derived as

$$M_e \dot{e}_d = J_e \big(M_u J_h^{-1} \Psi_1 + H_0 + W_1^T w - J_{\lambda_1}^T J_{\lambda_2}^{-T} J_{u_2}^T u_2 \big) \qquad (23)$$

where

$$J_e = \begin{bmatrix} I_2 & -M_c M_r^{-1} \end{bmatrix}; \quad M_e = M_s - M_c M_r^{-1} M_c^T. \qquad (24)$$

Here, M_e is symmetric positive definite, which is proven using equations that define the Schur complement: since $M_u = M_u^T > 0$, $M_e = M_s - M_c M_r^{-1} M_c^T = M_e^T > 0$. If M_e^{-1} is multiplied to both sides of the equation, we obtain $M_e^{-1} J_e = J_s M_u^{-1}$. The term J_e involves the coupled inertia at the floating base. While M_2 is a term that is relatively easy to acquire, M_1 is unknown and volatile as it can be affected by hand gestures and external loads. Therefore, J_e is extremely challenging to identify. However, from Eq.(10) it can be shown that

$$J_{e,u}^T = -J_s J_{\lambda_1}^T J_{\lambda_2}^{-T} J_{u_2}^T = -J_e J_{\lambda_1}^T J_{\lambda_2}^{-T} J_{u_2}^T \qquad (25)$$

This indicates that the inertia coupling effect does not affect u_2 if it is guaranteed that the current constraint structure holds. Since $J_{e,u}$ is a purely kinematic term, the controller design via u_2 can be realized if $J_{e,u}$ can be identified.

3.3 Stiffness and Tremor Dynamics

For the dynamic models introduced above, it is important to understand the possible source of tremor. To explain in a more general way, a final assumption is made based on the free base model to introduce stiffness into the system:

(A6) The term $M_u J_h^{-1} \Psi_1 + H_0$ has introduced stiffness into the system from muscle control signal [16] and passive stiffness [17], which leads to

$$M_u J_h^{-1} \Psi_1 + H_0 = M_u J_h^{-1} (-K_1 e_{1,p} - B_1 e_{1,d} + \Psi_{n,1}(x, e_1)) \qquad (26)$$

where $K_1,\ B_1 \in \mathbb{R}^{8\times 8}$ are respectively the state dependent stiffness and damping matrices that satisfy $K_1 = K_1^T > 0$ and $B_1 = B_1^T > 0$; $\Psi_n \in \mathbb{R}^8$ is the nonlinear stiffness and other internal stabilizing force effects that satisfy $\Psi_n(x, 0) = 0$.

Based on this assumption, Eq.(23) can be transformed into

$$M_e \dot{e}_d = -M_e (K_s e_p + B_s e_d) + H_{e,i} + J_e W_1^T w + J_{e,u}^T u_2 \qquad (27)$$

with

$$K_s = J_s K_1 J_s^T; \quad B_s = J_s B_1 J_s^T;$$
$$H_{e,i} = -M_e(J_s K_1 J_r^T J_r e_{1,p} + J_s B_1 J_r^T J_r e_{1,d}) + M_e J_s J_h^{-1} \Psi_{n,1}$$

Here $H_{e,i}$ is gross internal force that comes from the muscle control coupling input $-M_e(J_s K_1 J_r^T J_r e_{1,p} + J_s B_1 J_r^T J_r e_{1,p})$ and the nonlinear stiffness $M_e J_s J_h^{-1} \Psi_{n,1}$. Based on the aforementioned assumptions, the proposed error dynamic model is sufficient to simulate and test the effect of tremor controllers. A more accurate model can be obtained in the future by including the exact stiffness ratio between the neural signal and passive stiffness.

4 Wrist Kinematics Identification

Based on the dynamic analysis, it can be concluded that the combined system of the arm and TAWE has a lot of model uncertainties. The major uncertainties, apart from the inertia, also come from the unknown kinematic structure of the wrist. In addition to the characteristics of the wrist mentioned in Sec.1, the exoskeleton may be fixed at a different user arm location every time it is equipped. These kinematic uncertainties has made it extremely challenging to analyze and control the exoskeleton.

As mentioned previously, the controller can only work based on the condition that $J_{e,u}$ can be calculated. Here, a possible solution for the identification of wrist kinematics via nonlinear parameter estimation is proposed. The approach requires the design of a general kinematic structure to approximate the unknown wrist joint. In this study, the structure is designed based on the assumption that the wrist kinematics consists of a finite number of serial transformations as shown in Fig.5(a). Here, $T_{RUD}(\theta_{W,1})$ and $T_{FE}(\theta_{W,2})$ are pure rotational transformations based on the RUD and FE angles. Since the position and orientation of Frame #6 with respect to Frame #1 can be acquired from the exoskeleton kinematic chain, the unknown transformations are $T_{s1}(p_{d,1}, p_{r,1})$, $T_{s2}(p_{d,2}, p_{r,2})$, and $T_{s3}(p_{d,3})$, where $p_{d,1},\ p_{d,2},\ p_{d,3} \in \mathbb{R}^3$ are the unknown translation parameters, and $p_{r,1},\ p_{r,2} \in \mathbb{R}^3$ are the unknown rotation parameters in the form of Euler angle (which are assumed to be small rotations). Therefore, the unknown parameter vector is selected as

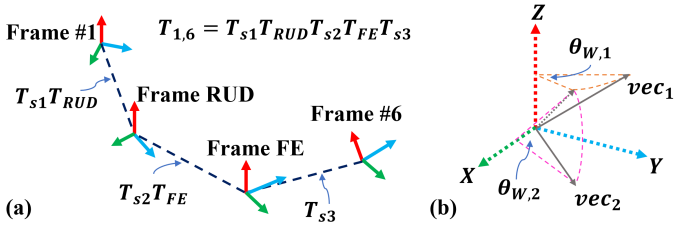

FIGURE 5: Demonstration of kinematic structures - (a): $T_{1,6}$ is assumed to be composed of T_{s1}, T_{RUD}, T_{s2}, T_{FE} and T_{s3}; (b): The orientation change of a directional vector on the hand from vec_1 to vec_2 can be realized with the $\theta_{W,1}$ (RUD) rotation around Z axis followed by the $\theta_{W,2}$ (FE) rotation around X axis in an arbitrary frame.

$$p = \begin{bmatrix} p_{d,1}^T & p_{d,2}^T & p_{d,3}^T & p_{r,1}^T & p_{r,2}^T \end{bmatrix}^T \tag{28}$$

In addition to the proposed uncertain kinematic structure, the regression requires the following assumptions:

(B1) The unknown parameters are constant/slow-varying and independent of the system states and other parameters.

(B2) The FE and RUD angles can be acquired as shown in Fig.5(b) (see explanation in the caption).

In the simulation, (B2) will not be applied as θ_W is assumed to be directly available.

4.1 Nonlinear Regression Objective and Algorithm

The identification of wrist kinematic is based on the measured translational displacement and velocity between the Frame #1 and Frame #5, and the estimated displacement and velocity through the kinematic structure. The data for the regression need to be collected overtime, which leads to the cost function designed as

$$\mathscr{J}(p) = \sum_{i=1}^{n} \alpha^{n-i} E_i^T \Omega E_i \tag{29}$$

The term $E_i = (z_i - \hat{z}_i)$ is the ith error data between the measured data z and the estimated data $\hat{z}$. In our case, $z = [\rho_{5,1}^T,\ \dot{\rho}_{5,1}^T]^T$ and $\hat{z} = [\rho_{5,2}^T(\theta_W, p),\ \dot{\rho}_{5,2}^T(\theta_W, \dot{\theta}_W, p)]^T$ (recall that $\rho_{5,1} = \rho_{5,2}$ from the constraint in Eq.(7)). Matrix $\Omega \in \mathbb{R}^{6\times 6}$ is a constant diagonal weight matrix. Finally, $\alpha \in (0, 1]$ is a forgetting factor to allow emphasis on the latest data for the parameter varying cases, which is set to $\alpha = 1$ when the parameters are assumed constant.

The basis of the current dynamic nonlinear parameter estimator is the Levenberg-Marquardt (LM) algorithm [18], which is a combination of the gradient descent and Gauss-Newton methods. For this case, the following modified version of LM update algorithm is adopted

$$p_{j+1} = p_j + h_j; \tag{30a}$$
$$\left(\sum_{i=1}^{n} \alpha^{n-i}\left(\Gamma_i + \beta_j \mathrm{diag}(\Gamma_i)\right)\right) h_j = \sum_{i=1}^{n} (\alpha^{n-i} J_{E,i}^T \Omega E_i) \tag{30b}$$

based on

$$J_{E,i} = \partial \hat{z} / \partial p; \quad \Gamma_i = J_{E,i}^T \Omega J_{E,i} \tag{31}$$

The above LM algorithm is characterized as "offline" in the sense that the step size h is updated based on the n sets of collected data. The damping parameter β_j is tuned so that the effect of the gradient descent elements will be prominent when p_j is resulting in poor estimation, while the effect of the Gauss-Newton elements will be prominent when p_j is close to a local minimum.

Compared to many other algorithms, LM algorithm is relatively simpler and more time-efficient in terms of calculation. In addition, the kinematic structure will provide the analytical expression of $J_{E,i}$, which is advantageous since the numerical

calculation of $J_{E,i}$ is avoided. While LM algorithm have certain limitations, it is a good option at the preliminary stage of the kinematic identification study.

4.2 Simulation of Parameter Estimation

The preliminary test of the parameter estimation is carried out in MATLAB simulation. The plant is modeled by adding complexity to the kinematic system in the CAD design. While the selection of the kinematic structure does not involve any state-dependent translations, such motions are modeled in the plant system. Therefore, the kinematic structural function will never be able to regress to the exact plant kinematics even though they are very similar. The evaluation procedure of the regression approach is listed below as:

(P1) A total of 50 sets of random continuous kinematic data of z are collected. The random trajectories are generated in a workspace of -75°$\sim$ 75°in FE and -20°$\sim$ 45°in RUD, each with a duration of 10 seconds. The sampling rate of the data is a practically achievable 250 Hz.

(P2) The data are post-processed by adding random noises of small amplitudes. The noise amplitude in the velocity data is higher than that in the displacement.

(P3) The nonlinear regression is carried out individually for each set of the data. All regressions starts from the same initial condition $p = 0_{15\times1}$. The MATLAB function `lsqcurvefit` is implemented in the LM mode with $\Omega = \text{diag}([1,1,1,0.2,0.2,0.2])$. The varying parameter is not considered in the evaluation by setting $\alpha = 1$.

Each set of the regressed parameter is then validated individually by every other set of the sampled data. Figure 6(a) presents the average performance of each individual set of p in estimating all other trajectories, which is measured by

$$\mathscr{K}_m = 0.02 \sum_{k=1}^{50} \left(\sum_{i=1}^{n} E_{d,i}^T \Omega E_{d,i} \right) \tag{32}$$

where $E_{d,i} = \rho_{5,1}(\theta_{W,k,i}, \dot{\theta}_{W,k,i}) - \rho_{5,2}(\theta_{W,k,i}, \dot{\theta}_{W,k,i}, p_m)$ is the position estimation error with the parameter from the mth regression on the ith data in the kth trajectory. The plot shows that performance cost of the parameters varies little between each two regressions. In this study, we can observe that $p_{d,1}$, $p_{d,2}$, and $p_{d,3}$ in every regression has reached the local minimums in the vicinity of the their average

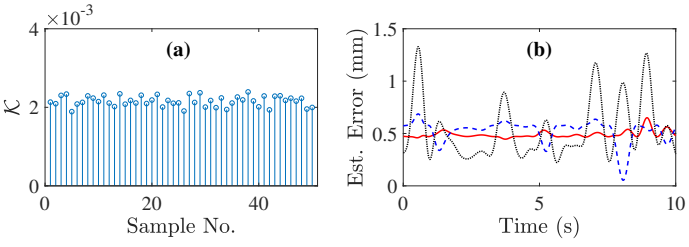

FIGURE 6: Performance of wrist kinematics estimation based on regressed parameters - (a): Average cost $\mathscr{K}$ of each individual set of p in estimating all trajectories; (b): The worst position estimation error case, where (1) solid line - error in X; (2) dash line - error in Y; (3) dot line - error in Z;

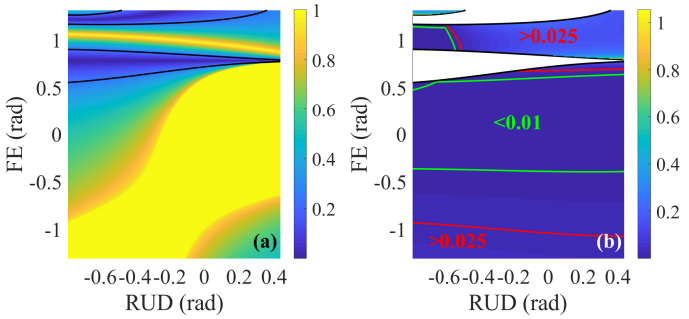

FIGURE 7: Analysis of $J_{e,u}$ and its estimation $\hat{J}_{e,u}$ - (a) map of eigenvalue real part magnitude ratio γ in the RUD-FE plane, where (1) black contour - $\gamma = 0.25$; (b): magnitude map of the δ in the selected RUD-FE area, where (1) black contour - $\gamma = 0.25$; (2) green contour - $\delta = 0.01$; (3) red contour - $\delta = 0.025$

$$\bar{p}_{d,1} = \begin{bmatrix} 6.7\text{e-}2 \\ 8.5\text{e-}2 \\ -1.4\text{e-}2 \end{bmatrix}; \; \bar{p}_{d,2} = \begin{bmatrix} -2.5\text{e-}3 \\ -5.0\text{e-}3 \\ -1.5\text{e-}2 \end{bmatrix}; \; \bar{p}_{d,3} = \begin{bmatrix} -2.2\text{e-}3 \\ 6.8\text{e-}2 \\ 6.3\text{e-}2 \end{bmatrix}$$

The cases with the largest deviation norms

$$\begin{aligned} \max(\{\|p_{d,1} - \bar{p}_{d,1}\|\}) &= 1.06\text{e-}3 \\ \max(\{\|p_{d,2} - \bar{p}_{d,2}\|\}) &= 1.10\text{e-}3 \\ \max(\{\|p_{d,3} - \bar{p}_{d,3}\|\}) &= 1.06\text{e-}3 \end{aligned}$$

are recorded in regression #9, #10, and #10 respectively. The variation in $p_{r,1}$ and $p_{r,2}$ is larger. This is likely due to the redundancy of the assigned unknown rotation parameters with respect to the kinematics of the plant system. Since the initial guess for all regressions are $p = 0_{15\times1}$, the uniformity in regressions has suggested the potential robustness of the LM method in such kinematic identification, under the condition that the estimated kinematic structure is similar to the actual kinematic structure. A future work is to explore a general and robust kinematic structure for actual human wrist based on (B2).

When analyzed and compared individually, the worst identification is discovered at the case when parameter from regression #9 is applied to estimate data #26 based on its wrist angle trajectories, which is shown in Fig.6(b). While the errors are relatively larger compared to the other cases, each of them did not exceed 2% of the maximum displacement range. It should also be reminded that the main purpose of nonlinear regression is to provide $\hat{J}_{e,u}(q,p)$ as the approximation of $J_{e,u}$, which is dependent on the position states of the system. An accurate estimation will yield

$$J_{e,u}\hat{J}_{e,u}^{-1} \sim I_2 \tag{33}$$

The characteristic of $J_{e,u}$ is first studied as shown in Fig.7(a) that

maps the ratio γ defined by

$$\gamma = |\kappa_1/\kappa_2|;\ \ \kappa_1,\kappa_2 \in \{\text{real}(\text{eig}(J_{e,u}))\};\ \kappa_1^2 < \kappa_2^2 \tag{34}$$

In the map, the areas where γ is small are close to singularity, which should be avoided during control and minimized during design optimization. The black contours on the map extract the acceptable area of $\gamma > 0.25$ for the analysis of δ defined as

$$\Delta = J_{e,u}\hat{J}_{e,u}^{-1} - I_2; \quad \delta = \max(\{|\Delta_{i,j}| \mid i = 1,2;\ j = 1,2\}) \tag{35}$$

where $\hat{J}_{e,u}$ is calculated with the p from regression #9. When δ is small, $J_{e,u}\hat{J}_{e,u}^{-1} \sim I_2$. The map in Fig.7(b) indicates that there are large areas where $J_{e,u}$ is well approximated by $\hat{J}_{e,u}$. It can be noticed that the $\hat{J}_{e,u}$ tends to be inaccurate near the singularity regions. Similar observations are achieved from the other regressed parameters. In general, $\hat{J}_{e,u}$ is acceptable when FE -75°$\sim$ 30°.

5 Control Framework and Simulation

The control framework that will be implemented on TAWE is illustrated in Fig.8. As previously discussed, the muscle input u_1 and disturbance/perturbation w in the forearm are assumed to come from the human user. The IMU sensors installed on the forearm will provide a coarse wrist joint measurement as $\theta_{W_{IMU}}$, which will be fused with θ_E by Kalman filter to provide a more accurate estimation θ_W. While θ_W will be used for wrist kinematic identification along with the $\rho_{5,1}$, it will also be fed into a voluntary motion filter (WFLC [10], EKF [11], etc.). The voluntary motion filter will also read other sensor signals such as EMG and EEG from the human user to extract the voluntary human wrist motion $\theta_{W,r}$. Together with the Jacobian estimation $\hat{J}_{e,u}$, the measurements and human intention will be used to generate control input u_2 into the actuators in TAWE. While modifications may apply to the framework in the future, the elements in the current framework are essential for any applications.

5.1 Controller Design

The controller design of the system is established on Eq.(27). In the equation, all the dynamic terms are assumed unknown. While model based controller require identification or estimation of these terms, the controller can be designed based on

$$\begin{aligned} u_2 = J_{e,u}^{-1}\big(&-k_i e_i - k_p e_p - k_d e_d - F_u(t,q,\dot{q})\hat{p}_u\big) \\ &+ \Phi(t,q,\dot{q},e,e_i) + w_u(t,q,\dot{q},e,e_i) \end{aligned} \tag{36}$$

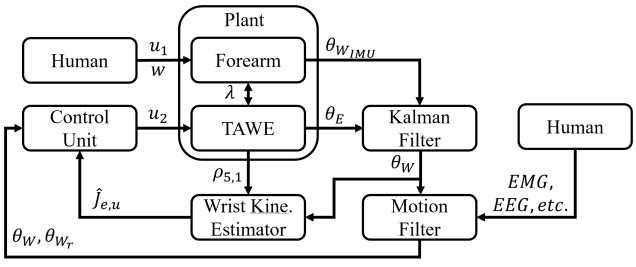

FIGURE 8: The control system framework of TAWE

where

$$e_i = \int_0^t e_p(\tau)d\tau \tag{37}$$

is the integral error e_i; $k_i, k_p, k_d > 0$ are PID control gains; $\hat{p}_u \in \mathbb{R}^{2\eta}$ is the adaptive control parameters as an estimation of the slow varying true value p_u (η is a positive integer); $F_u(t,q,\dot{q}) \in \mathbb{R}^{2\times 2\eta}$ is the adaptive control regressor matrix; $\Phi(t,q,\dot{q},e,e_i)$ includes the control term by other nonlinear methods; and $w_u(t,q,\dot{q},e,e_i) \in \mathbb{R}^2$ is the controller uncertainty due to the estimation $J_{e,u}$.

For the PID controller, to realize stabilization, the minimum requirement is to achieve the Hurwitz [19] state matrix

$$A_{PID} = \begin{bmatrix} 0 & I_2 & 0 \\ 0 & 0 & I_2 \\ -k_i M_e^{-1} & -k_p M_e^{-1} & -k_d M_e^{-1} \end{bmatrix} \tag{38}$$

Provided that the eigenvalues of M_e^{-1} are $\kappa_{m,1} > 0$ and $\kappa_{m,2} > 0$, the six eigenvalues κ_c of A_{PID} can be solved from the following equations

$$\begin{aligned} (\kappa_c^3 + k_d\kappa_{m,1}\kappa_c^2 + k_p\kappa_{m,1}\kappa_c + k_i\kappa_{m,1}) &= 0 \\ (\kappa_c^3 + k_d\kappa_{m,2}\kappa_c^2 + k_p\kappa_{m,2}\kappa_c + k_i\kappa_{m,2}) &= 0 \end{aligned} \tag{39}$$

According to Routh-Hurwitz criteria, the eigenvalues will have stable real parts when $k_d k_p \kappa_m > k_i$ for both $\kappa_{m,1}$ and $\kappa_{m,2}$. Therefore, the PID controller can only be applied with a good estimation of the range of κ_m, which is challenging when the user is performing multiple tasks. However, by setting $k_i = 0$, the PID controller will be simplified into the PD controller. The four eigenvalues of the state matrix of the PD controller

$$A_{PD} = \begin{bmatrix} 0 & I_2 \\ -k_p M_e^{-1} & -k_d M_e^{-1} \end{bmatrix} \tag{40}$$

can be calculated with

$$(\kappa_c^2 + k_d\kappa_{m,1}\kappa_c + k_p\kappa_{m,1})(\kappa_c^2 + k_d\kappa_{m,2}\kappa_c + k_p\kappa_{m,2}) = 0 \tag{41}$$

Therefore, there is no restriction from the Hurwitz property of A_{PD} on selecting the parameters for k_d and k_p.

Model reference adaptive controller (MRAC) is designed to counter the periodic tremor. By considering all the model terms as periodic system inputs identified within a known range of frequency, the equivalent gross input $F_u p_u$ can be constructed as

$$F_u p_u = \begin{bmatrix} \sum_{i=1}^{\eta} \big(\sin(\omega_i t)p_{u1,s,i} + \cos(\omega_i t)p_{u1,c,i}\big) \\ \sum_{i=1}^{\eta} \big(\sin(\omega_i t)p_{u2,s,i} + \cos(\omega_i t)p_{u2,c,i}\big) \end{bmatrix} \tag{42}$$

which is the combination of sinusoidal waves at ω_i from the identified frequency domain. This leads to the control system as

$$\dot{e} = A_{PD}e + \begin{bmatrix} 0 & M_e^{-1}(F_u p_u - F_u\hat{p}_u) \end{bmatrix}^T \tag{43}$$

The estimation parameter in the adaptive controller can then be updated as

$$\dot{\hat{p}}_u = -P_u^{-1}F_u^T e_d \tag{44}$$

with the symmetric positive definite gain update gain $P_u \in \mathbb{R}^{2\eta\times 2\eta}$ to stabilize the Lyapunov function

$$V = e_p^T e_p + e_d^T M_e e_d + (p_u - \hat{p}_u)^T P_u (p_u - \hat{p}_u) \qquad (45)$$

The application of the adaptive tremor controller, again, requires two conditions: (1) $\dot{M}_e \sim 0$ during the operation; (2) $\dot{p}_u \sim 0$; and (3) A_{PD} is positive definite. The first condition can be realized when the wrist angles do not change ferociously. The third condition requires $4k_p < k_d^2 \kappa_m$ for A_{PD}.

5.2 Simulation Study

Two simulation cases are studied to observe the characteristics of the controllers. The dynamic modeling via Kane's method [20] and the 3D simulation is carried out in a multibody toolbox [21] developed in MATLAB, as shown in Fig.9. While all controllers in the previous section require more or less some information in κ_m, the dynamic model based on common human parameter indicates that $\kappa_m > 100$ when there is no large inertia load on the wrist. This provides a relative large freedom to select the gains for various controllers. The simulation runs at 2500 Hz, while the control input rate is limited at 250 Hz for realistic concerns.

One simulation studies the light power augmentation by applying the PID controller to drive the wrist under zero muscle actuation. This simulation main intends to demonstrate the difference of the practical controller that adopts $\hat{J}_{e,u}$ from regression #9 and a ideal controller that adopts the true $J_{e,u}$. Here, we have selected $k_i = 0.25$, $k_p = 1$ and $k_d = 0.75$. The results in Fig.10 shows that the PID controller is able to keep up to the reference trajectory and maintain stability under small periodic disturbances. Apart from the disturbance, the error has not fully converge to zero also due to the lagging effect of the integral controller. It is also observed from the simulation that the maximum trajectory error between using $\hat{J}_{e,u}$ and $J_{e,u}$ are all below 1e-3 rad in non-disturbance simulation. This indicates that the uncertainty from the difference between the estimation and true value is trivial compared to the robustness of the PID controller.

The other simulation studies the tremor dynamics of the forearm. The disturbance consists of randomly generated sinusoidal inputs ranged from $4 \sim 8$ Hz. In practice, the frequency of the disturbance will be acquired with the voluntary motion filter.

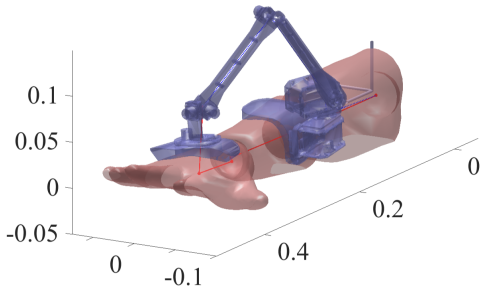

FIGURE 9: Simulation with 3D visualization in MATLAB (with axes units in meter)

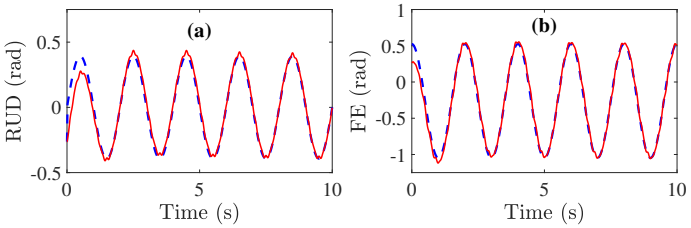

FIGURE 10: Trajectory tracking simulation with PID control (under small periodic disturbance) in (a): RUD and (b): FE, where (1) dash line - reference; (2) solid line - output)

The tremor of the system under no control, impedance control and adaptive control are compared in Fig.11. Notice that the impedance control has significantly reduced the amplitude of the tremor, while the adaptive control is able to counter almost all of the tremor after the parameters are converged. These observations suggest that the controller designs are feasible in simulation and has the potential to be applied in practical application.

6 Conclusion and Future Work

This paper introduces the dynamic analysis and control framework of the full wrist tremor alleviation exoskeleton TAWE. The multibody analysis has demonstrated a detailed dynamic system of study with the practical assumptions of human motion and tremor. The wrist kinematics identification approach is proposed and simulated to provide the potential feasibility in estimating $\hat{J}_{e,u}$, which is essential in realizing full control of the coupled wrist dynamics. The controller designs and their stability proofs are then presented and showcased with simulations. It should be noted that this complete framework of the dynamical analysis, kinematics identification, and control is general and can be applied to other cases of human wearable device design.

This study also suggests some future research directions:

(F1) While the dynamical structure of the system is proposed, the effect from the dynamical terms such as K_s, B_s, and $H_{e,i}$ has not been explored. Upcoming research will work on a full analysis of the system and study the effect from the parameter changes in these terms.

(F2) As Fig.7(a) indicates that the existence of singularity in $J_{e,u}$ has created obstacles in both kinematic identification and

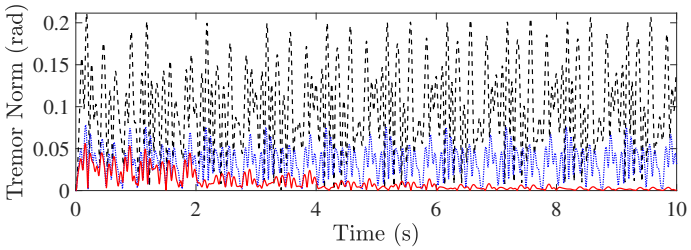

FIGURE 11: Tremor norm trajectories under different control suppression, where (1) black dash line - no suppression; (2) blue dot line - impedance (PD) control; (3) red solid line - MRAC active control

control, a major future design optimization objective will be eliminating the singularity in the workspace.

(F3) More dynamical property identification and control methods will be explored to attempt solving the coupling of dynamics terms in the controller, so that more functionalities can possibly be realized with the device.

Ultimately, TAWE will be prototyped and implemented in real life as a useful tool in helping to understand and control pathological tremors.

REFERENCES

[1] Limousin, P., Speelman, J., Gielen, F., Janssens, M., et al., 1999. "Multicentre european study of thalamic stimulation in parkinsonian and essential tremor". *Journal of Neurology, Neurosurgery & Psychiatry,* ***66***(3), pp. 289–296.

[2] Parkinson, J., 2002. "An essay on the shaking palsy". *The Journal of neuropsychiatry and clinical neurosciences,* ***14***(2), pp. 223–236.

[3] Hoehn, M. M., Yahr, M. D., et al., 1998. "Parkinsonism: onset, progression, and mortality". *Neurology,* ***50***(2), pp. 318–318.

[4] Markus Gnadinger, Hans-Ulrich Mellinghoff, A. K.-L., 2011. "Parkinsons disease and the bones". *Swiss Med Wkly,* ***141***, p. w13154.

[5] Pons, J. L., 2008. *Wearable robots: biomechatronic exoskeletons*. John Wiley & Sons.

[6] Loureiro, R. C., Belda-Lois, J. M., Lima, E. R., Pons, J. L., Sanchez-Lacuesta, J. J., and Harwin, W. S., 2005. "Upper limb tremor suppression in adl via an orthosis incorporating a controllable double viscous beam actuator". In Rehabilitation Robotics, 2005. ICORR 2005. 9th International Conference on, Ieee, pp. 119–122.

[7] Rocon, E., Belda-Lois, J., Ruiz, A., Manto, M., Moreno, J. C., and Pons, J., 2007. "Design and validation of a rehabilitation robotic exoskeleton for tremor assessment and suppression". *IEEE Transactions on Neural Systems and Rehabilitation Engineering,* ***15***(3), pp. 367–378.

[8] Huen, D., Liu, J., and Lo, B., 2016. "An integrated wearable robot for tremor suppression with context aware sensing". In 2016 IEEE 13th International Conference on Wearable and Implantable Body Sensor Networks (BSN), IEEE, pp. 312–317.

[9] Anouti, A., and Koller, W. C., 1995. "Tremor disorders. diagnosis and management.". *Western journal of medicine,* ***162***(6), p. 510.

[10] Riviere, C. N., Rader, R. S., and Thakor, N. V., 1998. "Adaptive cancelling of physiological tremor for improved precision in microsurgery". *IEEE Transactions on Biomedical Engineering,* ***45***(7), pp. 839–846.

[11] Bo, A. P. L., Poignet, P., and Geny, C., 2011. "Pathological tremor and voluntary motion modeling and online estimation for active compensation". *IEEE Transactions on Neural Systems and Rehabilitation Engineering,* ***19***(2), pp. 177–185.

[12] Li, Z.-M., Kuxhaus, L., Fisk, J. A., and Christophel, T. H., 2005. "Coupling between wrist flexion–extension and radial–ulnar deviation". *Clinical biomechanics,* ***20***(2), pp. 177–183.

[13] Aydoğ, E., Ekşioğlu, E., Çakci, A., and Yilmaz, Ö., 2005. "Hand deformity in parkinsons disease: case report". *Rheumatology international,* ***25***(7), pp. 548–549.

[14] Moore, D. C., Crisco, J. J., Trafton, T. G., and Leventhal, E. L., 2007. "A digital database of wrist bone anatomy and carpal kinematics". *Journal of biomechanics,* ***40***(11), pp. 2537–2542.

[15] Fresk, E., and Nikolakopoulos, G., 2013. "Full quaternion based attitude control for a quadrotor". In Control Conference (ECC), 2013 European, IEEE, pp. 3864–3869.

[16] Wu, D., Warwick, K., Ma, Z., Gasson, M. N., Burgess, J. G., Pan, S., and Aziz, T. Z., 2010. "Prediction of parkinson's disease tremor onset using a radial basis function neural network based on particle swarm optimization". *International journal of neural systems,* ***20***(02), pp. 109–116.

[17] Formica, D., Charles, S. K., Zollo, L., Guglielmelli, E., Hogan, N., and Krebs, H. I., 2012. "The passive stiffness of the wrist and forearm". *American Journal of Physiology-Heart and Circulatory Physiology*.

[18] Marquardt, D. W., 1963. "An algorithm for least-squares estimation of nonlinear parameters". *Journal of the society for Industrial and Applied Mathematics,* ***11***(2), pp. 431–441.

[19] Skogestad, S., and Postlethwaite, I., 2007. *Multivariable feedback control: analysis and design*, Vol. 2. Wiley New York.

[20] Kane, T. R., and Levinson, D. A., 1983. "The use of kane's dynamical equations in robotics". *The International Journal of Robotics Research,* ***2***(3), pp. 3–21.

[21] Wang, J., Kamidi, V. R., and Ben-Tzvi, P., 2018. "A multibody toolbox for hybrid dynamic system modeling based on nonholonomic symbolic formalism". In ASME 2018 Dynamic Systems and Control Conference, American Society of Mechanical Engineers, pp. V003T29A003–V003T29A003.